International Journal of Surface Science and Engineering

ISSN online: 1749-7868 - ISSN print: 1749-785X
https://www.inderscience.com/ijsurfse

Influence of temperature on the metallic surface cleanliness in ICF facility: a combined experimental and molecular simulation study

Yilan Jiang, Longfei Niu, Guorui Zhou, Xinxiang Miao, Haibin Lv, Wen Qian

DOI: 10.1504/IJSURFSE.2023.10051543

Article History:
Received: 04 July 2022
Accepted: 06 September 2022
Published online: 08 February 2023

Influence of temperature on the metallic surface cleanliness in ICF facility: a combined experimental and molecular simulation study

Yilan Jiang, Longfei Niu, Guorui Zhou, Xinxiang Miao, Haibin Lv and Wen Qian*

China Academy of Engineering Physics,
Mianyang, 621900, China
Email: jiangyilan1023@163.com
Email: niulf@caep.cn
Email: zhougr@caep.cn
Email: miaoxinxiang.714@163.com
Email: haibinglv@163.com
Email: qianw03@caep.cn
*Corresponding author

Abstract: Wettability of metal surfaces is used to characterise the surface cleanliness of components in the inertial confinement fusion (ICF) facility. In this work, molecular simulations combined with wettability experimentation were performed. The temperature effects of water-metallic interface energies and their influence on the measurements for surface cleanliness were investigated. The simulation results indicated van der Waals forces promoted the attraction between water molecules and metal surfaces. The interaction energies raised with elevated temperatures from 291 K to 303 K. Besides, the wettability experiments showed both the Al and Fe components were hydrophilic, and the contact angle was reduced with elevated temperatures. The correlationship between the energy change and the contact angle at varying temperatures can be found. This research provides a new understanding of the characterisation of metal surface cleanliness.

Keywords: surface cleanliness; solid-liquid interface; contact angle test; molecular dynamics.

Reference to this paper should be made as follows: Jiang, Y., Niu, L., Zhou, G., Miao, X., Lv, H. and Qian, W. (2023) 'Influence of temperature on the metallic surface cleanliness in ICF facility: a combined experimental and molecular simulation study', *Int. J. Surface Science and Engineering*, Vol. 17, No. 1, pp.30–43.

Biographical notes: Yilan Jiang is an Assistant Research Fellow in the China Academy of Engineering Physics, Mianyang, China. Her fields of interest are in materials surface cleanliness test and laser technology.

Longfei Niu is an Assistant Research Fellow in the China Academy of Engineering Physics, Mianyang, China. His fields of interest are in materials surface modification and test.

Guorui Zhou is an Associate Research Fellow in the China Academy of Engineering Physics, Mianyang, China. His fields of interest are in materials surface theory and tests.

Xinxiang Miao is an Associate Research Fellow in the China Academy of Engineering Physics, Mianyang, China. His fields of interest are in materials cleanliness theory and tests.

Haibin Lv is a Senior Engineer in the China Academy of Engineering Physics, Mianyang, China. His fields of interest are in materials tests and laser engineering.

Wen Qian is an Assistant Research Fellow in the China Academy of Engineering Physics, Mianyang, China. His fields of interest are in molecular modelling and characterisations.

1 Introduction

Cleanliness is an important factor limiting the increase in output power in inertial confinement fusion (ICF) facilities (Pryatel et al., 2014; Li et al., 2022a). The metal components take up more than 80 % of the components in the ICF facilities and directly contact the large-aperture optics. The damage threshold of the optical components decreases significantly due to the particles and aerosols sputtered from the contaminated surface of metal components under the action of high-energy lasers (Yin et al., 2022; Yin and Cao 2019; Muñoz et al., 2017). Therefore, the surface cleanliness of metal components is of great significance to protecting optical components and the stable operation of facilities.

The commonly-used metal components in ICF facilities are consisted of the stainless steel 304 or aluminium alloy 6061, with main elements Fe or Al. The wettability measurements are used to characterise the surface cleanliness of these metals (Li et al., 2022b, 2011). The surface cleanliness is related to the wetness degree of water on the surfaces, and the angle between the tangent line of the gas-liquid interface and solid-liquid boundary, namely the contact angle, can determine the wetness (Trevoy and Johnson, 1958; Erb, 1965; Gim et al., 2019). For example, if the water contact angle is less than 90°, the materials are hydrophilic and could be regarded as clean. In contrast, the surface shows hydrophobic, which may be contaminated by organic contaminants and other impurities (Pryatel et al., 2014; Li et al., 2022a). The change of intermolecular interaction at the interface is the main reason for the evolution of wettability, which is sensitive to thermodynamic temperatures (Deng et al., 2022; Sobczak et al., 2005; Emelyanenko et al., 2020). Consequently, temperature effects should be considered to investigate the interface interactions and obtain precise cleanliness results.

In recent years, molecular dynamics (MD) simulations have shown great ability in investigating solid-liquid interfaces at the atomic level, such as water-metallic interfaces (Li et al., 2022b, 2020; Das et al., 2020). The stable interface structures and interface energies have been well represented using MD (Li et al., 2020) or density functional theory (Das et al., 2020). In this work, a combined strategy of molecular modelling and wettability experiment was carried out to explore the temperature effects of water-metallic interface energies and their influence on the cleanliness experiments.

2 Methodology

2.1 Molecular simulations

Water-metallic interface models were constructed to investigate the interface interaction energies for water on the metals at the temperatures 291–303 K. The amorphous cells (AC) of water (H_2O) were established with a density of 1.0 g/cm^3, where the short lines between H and O atoms represent the chemical bonds in the water molecule. We use the crystalline structure of the main element Al or Fe to describe the metallic samples, where Al crystal is in fcc stacking style, fm-3m space group, with cell parameters $a = b = c = 0.405$ nm, $\alpha = \beta = \gamma = 90°$ (Cai and Ye, 1996). Fe crystal is in bcc stacking style, im-3m space group, with cell parameters $a = b = c = 0.28664$ nm, $\alpha = \beta = \gamma = 90°$ (Sun et al., 2004). The neighbour atoms have metallic bonds represented by the potential field's atomic interactions. Considering the existence of the H_2O molecular system, the COMPASS force-field (Sun et al., 1998; Sun, 1998) was applied, which can cover the interactions between H, O, Fe, and Al elements. Considering the anisotropy of the metallic crystals, the supercells of 5 × 5 × 5 Al and 10 × 10 × 10 Fe were cut along (1 0 0), (1 1 0), and (1 1 1), respectively. These surfaces were assumed to be atomically smooth in the atomic simulations, because in such micro-scale, the surface roughness can not be present. On the other hand, the influence of surface roughness were explained using experimental tests (Figure A2). The amorphous cells containing 200 H_2O molecules were put onto each metallic surface to form water-metallic (liquid-solid) interface models, along with a 2 nm vacuum layer on the top to overcome the influence of the upper interface. Compared with other interface models (Ghoufi et al., 2016; Di et al., 2021), the vacuum layer efficiently describes the water molecules on top of metal surfaces. Before adding onto the metal surface, the amorphous water cells had been optimised. After the water molecules are put on the metal surfaces, the whole interface models were optimised using molecular mechanics (MM) (Verlet et al., 1967; Ermer, 1976) using a cascade algorithm of the steepest descent (Levitt and Lifson, 1969). Adjusted basis set Newton-Raphson and quasi-Newton methods (Ermer, 1976), and the convergence thresholds are 2×10^{-5} kcal/mol in energy, 0.001 GPa in stress and 1×10^{-5} in displacement. The constructed H_2O/Fe interface model is as shown in Figure 1, and a similar H_2O/Al interface model is as shown in Figure A1.

To equilibrate the temperature of the systems and compare the temperature effects, MD simulations were carried out under COMPASS force-filed using NVT ensemble (constant particle number, volume and temperature), with varying temperatures 291 K, 296 K, 297 K, 298 K, 299 K, 300 K, 301 K, 302 K and 303 Nosé et al. (1984a, 1984b, 1991) method was used to control the temperatures. The van der Waals forces were summed by the atom-based method, while the Ewald et al. (1921) and Karasawa and Goddard (1989) method calculated the electrostatic forces. Three replica simulations are carried out for each system to reduce random errors. Each MD simulation lasts 1 ns (1,000 ps) to ensure the equilibrium of both temperature and energy (Figure 2).

Figure 1 Atomic model for the water-metallic interface: H_2O-Fe(1 0 0) is taken as an example, and Fe, H, and O atoms are represented using dark blue, white, and red colours, respectively (see online version for colours)

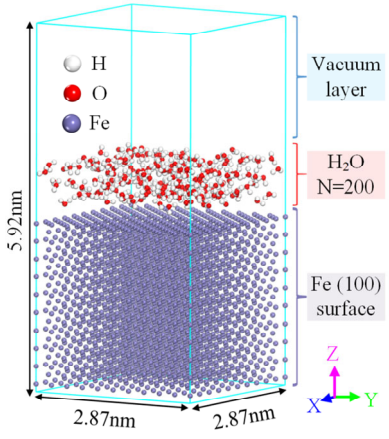

Figure 2 Time evolution of potential energy, kinetic energy, non-bond energy and total energy for H_2O-Al(1 0 0) interface model at 300 K (see online version for colours)

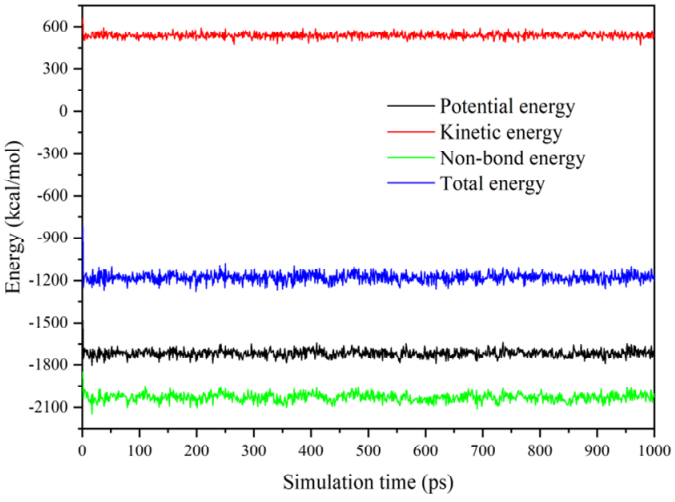

2.2 Experimental tests

The contact angle tests were carried out on the metal components to validate the surface interactions and determine the surface cleanliness of these components (Stalder et al., 2006; Lee et al., 2008; Stalder et al., 2010; Matykina et al., 2011). The portable contact angle tester (MobileDrop, KRÜSS GmbH) was used in all the measurements, which is accurate, portable and efficient. The tester has its own injector to drop liquid on the surface of the sample, with an accuracy of 2 µl. The stainless steel 304 (with main element Fe) and aluminium alloy 6061 (with main element Al) are chosen as the samples of the tests to simulate the components of the high-power laser facility, and both samples

are in the same dimension of 100 × 100 × 10 mm. Before the surface tests, a clean treatment process was carried out on each sample. Firstly the sample was infiltrated in high-pressure water for 10 min, and in cleaning agent for another 10 min; then it was washed under high-pressure water for three times, dried under ethyl alcohol, and dried by heating for four hours. Finally, the surface test experiments are carried out on the treated samples under various temperatures as the molecular simulations from 291–303 K at a constant humidity of 40% RH. Thus, the contact angles at elevated temperatures were obtained (Li et al., 2007; Hung et al., 2010).

The above experimental works had been carried out on the samples with same surface roughness, in order to find the influence of temperature with other factors be the same. Besides, additional experiments had been performed to explain the effect of surface roughness as shown in Appendix 2. The results show that the contact angles for both Al and Fe reduce with elevated surface roughness, which is consistent with the Wenzel (1936) model.

3 Results and discussion

3.1 Anisotropy of interface interactions

During the MD simulation, the H_2O were absorbed onto the metallic surface. As shown in Figure 3, in which the snapshots for H_2O-Fe(1 0 0) interface model at 298 K were taken for example, almost all of the H_2O molecules were on the metallic surface at 200 ps, and the system were equilibrated from 200 ps to 1,000 ps. The equilibrium trajectories were used to analyse the interaction energy (E_{inter}), which is the difference between the energy of the total system (E_{total}) and the divided systems, including the metallic surface (E_{metal}) and the water AC (E_{water}), normalised by the contact surface area (S) [equation (1)], and the contributions of van der Waals force (*vdW*) and electrostatic force (*ES*) were also calculated as shown in Table 1, where the '*other*' energy term contains long range correction and other energy except for *vdW* and *ES* energies. From the results of three replica simulations for each system, it can be seen that the calculated energies remain the same for each system at a specific temperature and pressure.

$$E_{inter} = \left[E_{total} - \left(E_{metal} + E_{water}\right)\right] / S \tag{1}$$

It can be concluded from Table 1 that the water molecules have attractive interactions (negative interaction energy values) with the metallic surfaces, in which the van der Waals forces contribute most, long range corrections and other energies also contribute (Oss et al., 1988; Kwok, 1999; Oss, 2002; Zhao, 2002). In contrast, the electrostatic forces are relatively small because the electrostatic interactions mainly exist between H_2O molecules.

The more negative interaction energy value is, the stronger the attractive interaction energy will be. For different metals, the interactions are different, in which water on the Fe template is stronger. For Fe surfaces, the absolute values of interaction energies are all larger than 60 kcal/mol per nm^2, while Al surfaces are all smaller than 50 kcal/mol per nm^2.

Table 1 Interaction energies and their components for water on different metallic surfaces at elevated temperatures from 291–303 K

System	*T/K*	E_{inter}/[kcal/(mol·nm^2)]	*van der Waals/* [kcal/(mol·nm^2)]	*Electrostatic/* [kcal/(mol·nm^2)]	*Other/*[kcal/(mol·nm^2)]
H_2O-Al(100)	291	–40.0706	–38.5622	–0.0002	–1.5082
	296	–41.3951	–39.8867	–0.0002	–1.5081
	297	–42.0053	–40.4972	–0.0002	–1.5078
	298	–42.3283	–40.8202	–0.0002	–1.5078
	299	–42.4785	–40.9702	–0.0002	–1.5081
	300	–43.9105	–42.4023	–0.0002	–1.5079
	301	–44.3821	–42.8738	–0.0002	–1.5081
	302	–44.6846	–43.1765	–0.0002	–1.5078
	303	–45.8852	–44.3771	–0.0002	–1.5079
H_2O-Al(110)	291	–37.9700	–36.8615	–0.0003	–1.1081
	296	–38.2111	–37.1026	–0.0003	–1.1081
	297	–38.3729	–37.2644	–0.0003	–1.1081
	298	–38.4481	–37.3396	–0.0003	–1.1081
	299	–39.2913	–38.1827	–0.0003	–1.1083
	300	–39.9504	–38.8419	–0.0003	–1.1081
	301	–40.0860	–38.9775	–0.0003	–1.1081
	302	–40.1396	–39.0310	–0.0003	–1.1082
	303	–40.3169	–39.2085	–0.0003	–1.1081
H_2O-Al(111)	291	–33.9964	–33.1547	–0.0002	–0.8414
	296	–34.0626	–33.2211	–0.0002	–0.8413
	297	–34.2182	–33.3767	–0.0002	–0.8413
	298	–34.5937	–33.7522	–0.0002	–0.8413
	299	–34.6348	–33.7932	–0.0002	–0.8413
	300	–35.6658	–34.8243	–0.0002	–0.8413
	301	–35.9210	–35.0794	–0.0002	–0.8413
	302	–36.1461	–35.3047	–0.0002	–0.8412
	303	–36.1522	–35.3107	–0.0002	–0.8413
H_2O-Fe(100)	291	–90.0349	–88.3487	–0.0004	–1.6858
	296	–90.2023	–88.5162	–0.0004	–1.6858
	297	–90.2905	–88.6043	–0.0004	–1.6858
	298	–90.4620	–88.7758	–0.0004	–1.6858
	299	–91.0227	–89.3365	–0.0004	–1.6858
	300	–91.1630	–89.4768	–0.0004	–1.6858
	301	–91.1664	–89.4802	–0.0004	–1.6857
	302	–91.9536	–90.2673	–0.0004	–1.6859
	303	–92.1917	–90.5055	–0.0004	–1.6858

Table 1 Interaction energies and their components for water on different metallic surfaces at elevated temperatures from 291–303 K (continued)

System	*T/K*	E_{inter}/[kcal/(mol·nm^2)]	*van der Waals/* [kcal/(mol·nm^2)]	*Electrostatic/* [kcal/(mol·nm^2)]	*Other/*[kcal/(mol·nm^2)]
H_2O-Fe(110)	291	–81.5840	–80.3273	–0.0003	–1.2564
	296	–82.4305	–81.1737	–0.0003	–1.2565
	297	–82.5717	–81.3148	–0.0003	–1.2565
	298	–82.7999	–81.5431	–0.0003	–1.2565
	299	–83.4921	–82.2353	–0.0003	–1.2564
	300	–83.5101	–82.2533	–0.0003	–1.2564
	301	–83.8524	–82.5957	–0.0003	–1.2564
	302	–84.7604	–83.5035	–0.0003	–1.2565
	303	–84.7658	–83.5090	–0.0003	–1.2565
H_2O-Fe(111)	291	–63.7328	–62.8385	–0.0003	–0.8939
	296	–63.8278	–62.9336	–0.0003	–0.8939
	297	–64.0710	–63.1768	–0.0003	–0.8939
	298	–64.1787	–63.2845	–0.0003	–0.8939
	299	–64.2775	–63.3833	–0.0003	–0.8939
	300	–64.6729	–63.7787	–0.0003	–0.8939
	301	–65.0172	–64.1230	–0.0003	–0.8939
	302	–65.1140	–64.2198	–0.0003	–0.8939
	303	–65.7512	–64.8570	–0.0003	–0.8940

Figure 3 Snapshots of transient atomic positions versus time for H_2O-Fe(1 0 0) interface model at 300 K (see online version for colours)

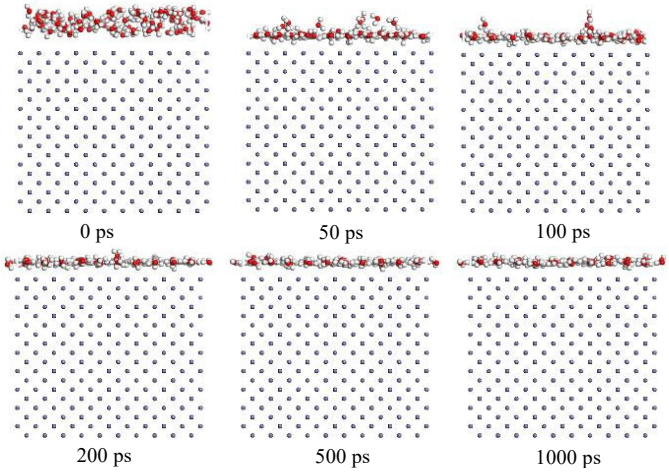

For the same metal, the interactions show anisotropy along different crystalline directions, for water on Al (1 0 0) > (1 1 0) > (1 1 1), while for water on Fe (1 0 0) > (1 1 0) > (1 1 1). For H_2O/Fe interfaces, the absolute value of interaction energy of

H_2O/Fe(1 0 0) interface is the largest, thus the interactions at H_2O/Fe(1 0 0) interface is the strongest. This is caused by the different surface density along different crystalline directions: if we extract the close contact surface of each crystalline direction (we take the depth of 0.3 nm for each surface for example), the surface density can be calculated by the total atom number times the total volume of the contact surface, the results are as shown in Table 2. It can be seen that the surface density of Fe(1 0 0) is largest, which means that more Fe atoms can interact with H_2O molecules at the interface, resulting larger interaction energy in this direction.

Table 2 Surface density for Fe contact surfaces along different directions

Contact surface	*Total atom number*	*Total volume [nm³]*	*Surface density [nm⁻³]*
Fe(1 0 0)	342	2.866 × 2.866 × 0.3	138.788
Fe(1 1 0)	441	2.866 × 4.054 × 0.3	126.519
Fe(1 1 1)	442	4.054 × 4.054 × 0.3	89.647

Above all, the attractive forces between water and Al or Fe metallic surfaces are strong, making the samples a hydrophilic material. The surface tension and contact angle between water and these materials are expected to be small (Mitroy and Zhang, 2007).

3.2 Temperature effects on interaction energies

It should be noted that the absolute values of interaction energies raised with the temperature from 291 K to 303 K (Figure 4). Under NVT ensemble which has a fixed particle number and system volume, the kinetic energy of H_2O molecules raised with the elevated temperatures (Klotz and Rusenberg, 2008), thus the movements of H_2O molecules exacerbated, and more H_2O molecules were possible to contact with the metallic surfaces, considering the contact surface area is the same for each interface model, the interactions for more molecules with the surface were computed if temperature raised, resulting in the increase of the interface energy, which mainly contributed by van der Waals forces.

Figure 4 The interaction energies as functions of temperatures for different surfaces (see online version for colours)

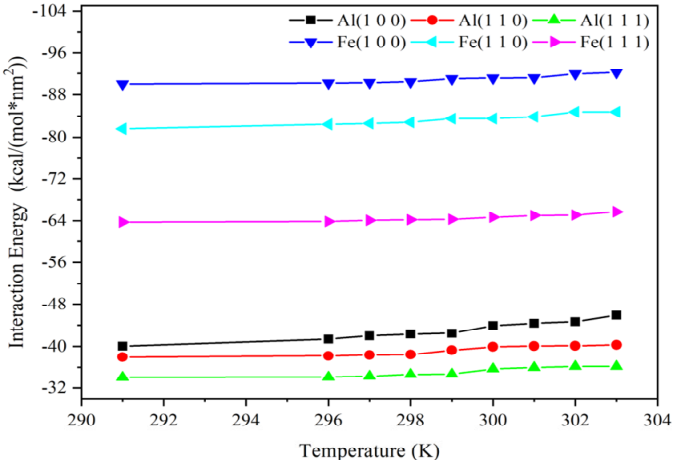

Table 3 Interaction energy gradient at elevated temperatures from 291–303 K

System	*Energy gradient [kcal/(mol·nm²·K)]*	*System*	*Energy gradient [kcal/(mol·nm²·K)]*
H_2O-Al (1 0 0)	0.4824	H_2O-Fe (1 0 0)	0.1880
H_2O-Al (1 1 0)	0.2355	H_2O-Fe (1 1 0)	0.2813
H_2O-Al (1 1 1)	0.2216	H_2O-Fe (1 1 1)	0.1643

The energy gradients at elevated temperatures can be found by correlating the absolute values of interaction energies with temperatures. The values of energy gradient for each system are summed in Table 3, from which it can be seen that the energy gradients for water on both Al and Fe show anisotropy. With the elevated temperature, the attractive interactions between water and metal surfaces increased, and on different surfaces, the increasing attractive forces show slight differences.

3.3 Correlation interface interactions to contact angles

The results of the contact angle tests at various temperatures from 291 K to 303 K and a constant humidity of 40 % RH were analysed. In the experiments, for each sample, two different test points on the surface were chosen to do in situ tests. For each point, ten parallel tests of contact angle were performed to reduce the random error. The average values of the results were calculated as shown in Figure 5.

Figure 5 The experimental contact angle as functions of test temperatures (see online version for colours)

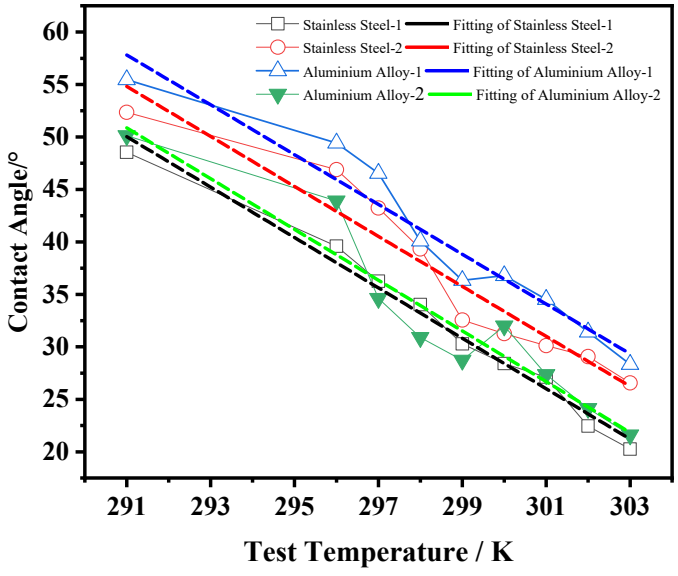

As a result, the contact angles for both Al and Fe samples are all small (<60°), in the range for hydrophilic materials, which match with the calculation results of strong surface energies. In addition, for both samples, the contact angles reduce with elevated temperatures from 291 K to 303 K. Linear relationship can be found for each test with

correlation coefficients all larger than 0.90, and the standard error (*e*), residual sum of squares (*RSS*), and adj. R-square (R^2) for the linear fitting of the contact angle test points are summarised in Table 4. Then the contact angle gradient at elevated temperatures can be derived from the slope value average, and the results are –2.3962°/K for Al, and –2.3920°/K for Fe. It can be seen that the contact angle gradients for the Al sample and Fe sample are all around the value of –2.4°/K, with slight changes caused by the different test points. The changes in contact angle also match with the surface energy gradients, proving that with elevated temperature, the atomic and molecular movements exacerbated; as proved by the snapshots of our simulations (Figure 3), more and more water molecules can contact with the metallic surfaces with elevated temperatures, causing the sum of interface interactions increase; finally, the surface energy rise, causing the reduction of surface tension and contact angle (Rubio et al., 2000). It can be concluded that the experiments consisted of computations.

Table 4 Standard error, RSSs and R^2 for linear fitting of the contact angle test points

System	*Intercept*	*e*	*Slope*	*e*	*RSS*	R^2
Fe sample 1	93.2680	2.9120	–2.4020	0.1129	9.4832	0.9826
Fe sample 2	97.6931	6.4494	–2.3819	0.2501	46.5167	0.9181
Al sample 1	100.5413	5.6193	–2.3737	0.2179	35.3129	0.9363
Al sample 2	94.4063	7.0688	–2.4187	0.2741	55.8793	0.9057

The above proved the quantitative combination of MD simulation with experimental results, the energy gradient with elevated temperatures was calculated by simulations, while the contact angle gradient at elevated temperatures was derived from experimental tests, thus we explained the influence of temperatures with quantitative results.

4 Conclusions

Combined methods of experimental tests and molecular simulations were conducted to investigate the temperature effects of interface interactions for water on metallic surfaces. Conclusions can be found as follows:

Firstly, there are strong, attractive forces between water molecules and metallic surfaces; the interactions are different for different metals. The interaction energies between water and Fe are stronger than that of Al; for the same metal, the interactions show anisotropy and different crystalline directions.

Moreover, the absolute values of interaction energies raised with temperatures, and the energy gradient at elevated temperatures is isotropic.

Meanwhile, the experimental tests show that the contact angle is relatively small, proving the metallic surfaces to be hydrophilic. What's more, the contact angle reduces with elevated temperatures. The contact angle gradient versus temperatures are obtained thorough linear fitting. Furthermore, correlation was found between the contact angle gradient and the surface energy gradient.

The above shows that temperatures positively affect water-metallic interface energies. In accurate contact angle tests for the cleanliness of high-power-laser facilities, these conclusions about temperature effects should be considered: temperature is a very general influential factor in manufacturing high-quality surfaces requiring high surface

cleanliness, and we explain this effect using the essential energy changes. It can be found that the energy gradient is different for different materials surface, in that case, this work have also provide a way to find the influential factor for surface cleanliness considering the essential energy nature of materials.

Acknowledgements

The authors acknowledge the support from the National Natural Science Foundation of China (NSFC) (Grant Nos. 61605186, 61705205 and 51535003) and China Scholarship Council (Grant No. 201904890009). Thanks for the attentive suggestions from the reviewers.

References

Cai, J. and Ye, Y.Y. (1996) 'Simple analytical embedded-atom-potential model including a long-range force for fcc metals and their alloys', *Phys. Rev. B*, Vol. 54, No. 12, p.8398.

Das, P., Rout, B. and Manju, U. (2020) 'Tunable wettability and conductivity of the graphene oxide surface with insights from density functional theory and molecular dynamics investigations', *J. Phys. Chem. C*, Vol. 124, No. 19, pp.10541–10549.

Deng, J., Song, Y. and Lan, Z. (2022) 'The surface modification effect on the interfacial properties of glass fiber-reinforced epoxy: a molecular dynamics study', *Nanotechnology Reviews*, Vol. 11, No. 1, p.1143.

Di, J.W., Yang, Z. and Duan, Y.Y. (2021) 'Molecular dynamics simulation on spreading of mixture nanodroplets on a smooth and homogeneous surface', *AIP Adv.*, Vol. 11, No. 4, p.45104.

Emelyanenko, K.A., Emelyanenko, A.M. and Boinovich, L.B. (2020) 'Water and ice adhesion to solid surfaces: common and specific, the impact of temperature and surface wettability', *Coatings*, Vol. 10, No. 7, p.648.

Erb, R.A. (1965) 'Wettability of metals under continuous condensing conditions', *J. Phys. Chem.*, Vol. 69, No. 4, p.1306.

Ermer, O. (1976) 'Calculation of molecular properties using force fields. Applications in organic chemistry', *Struct. Bond.*, Vol. 27, pp.161–211.

Ewald, P.P. (1921) 'Die Berechnung optischer und elektrostatischer gitter potentiale (the calculation of optical and electrostatic lattice potentials)', *Ann. Phys. Leipzig.*, Vol. 64, p.253.

Ghoufi, A., Malfreyt, P. and Tildesley, D.J. (2016) 'Computer modelling of the surface tension of the gas-liquid and liquid-liquid interface', *Chem. Soc. Rev.*, Vol. 45, No. 5, pp.1387–1409.

Gim, S., Cho, K.J. and Lim, H.K. (2019) 'Structure, dynamics, and wettability of water at metal interfaces', *Sci. Rep.*, Vol. 9, No. 1, p.1.

Hung, Y.L., Chang, Y.Y., Wang, M.J. and Lin, S.Y. (2010) 'A simple method for measuring the superhydrophobic contact angle with high accuracy', *Review of Scientific Instruments*, Vol. 81, No. 6, p.65105.

Karasawa, N. and Goddard, W.A. (1989) 'Acceleration of convergence for lattice sums', *J. Phys. Chem.*, Vol. 93, pp.7320–7327.

Klotz, I.M. and Rusenberg, R.M. (2008) *Chemical Thermodynamics: Basic Theory and Methods*, pp.29–41, John Wiley & Sons, Inc., New Jersey.

Kwok, D.Y. (1999) 'The usefulness of the Lifshitz-van der Waals/acid-base approach for surface tension components and interfacial tensions', *Colloids & Surfaces A: Physicochemical & Engineering Aspects*, Vol. 156, No. 1, pp.191–200.

Lee, B., Ravindra, P. and Chan, E. (2008) 'A critical review: surface and interfacial tension measurement by the drop weight method', *Chem. Eng. Comm.*, Vol. 195, No. 7, pp.889–924.

Levitt, M. and Lifson, S. (1969) 'Refinement of protein conformations using a macromolecular energy minimization procedure', *J. Mol. Biol.*, Vol. 46, p.269.

Li, D., Xiong, M. and Wang, S. (2020) 'Effects of low-temperature plasma treatment on wettability of glass surface: molecular dynamic simulation and experimental study', *Appl. Surf. Sci.*, Vol. 503, p.144257.

Li, X.M., Reinhoudt, D. and Crego-Calama, M. (2007) 'What do we need for a superhydrophobic surface? A review on the recent progress in the preparation of superhydrophobic surfaces', *Chem. Soc. Rev.*, Vol. 36, No. 8, pp.1350–1368.

Li, Y., Bai, Q. and Guan, Y. (2022a) 'In situ plasma cleaning of large-aperture optical components in ICF', *Nuclear Fusion*, Vol. 62, No. 7, p.076023.

Li, Y., Bai, Q. and Yao, C. (2022b) 'Long-lasting antifogging mechanism for large-aperture optical surface in low-pressure air plasma in-situ treated', *Appl. Surf. Sci.*, Vol. 581, p.152358.

Liu, K. and Jiang, L. (2011) 'Metallic surfaces with special wettability', *Nanoscale*, Vol. 3, No. 3, p.825.

Matykina, E., Garcia, I., Damborenea, J.J.D. and Arenas, M.A. (2011) 'Comparative determination of TiO_2 surface free energies for adhesive bonding application', *International Journal of Adhesion & Adhesives*, Vol. 31, No. 8, pp.832–839.

Mitroy, J. and Zhang, J.Y. (2007) 'Long-range dispersion interactions. II. Alkali-metal and rare-gas atoms', *Phys. Rev. A*, Vol. 76, p.32706.

Muñoz, J., Bravo, J.A. and Calzada, M.D. (2017) 'Aluminum metal surface cleaning and activation by atmospheric-pressure remote plasma', *Appl. Surf. Sci.*, Vol. 407, p.72.

Nosé, S. (1984a) 'A molecular dynamics method for simulations in the canonical ensemble', *Mol. Phys.*, Vol. 52, pp.255–268.

Nosé, S. (1984b) 'A unified formulation of the constant temperature molecular dynamics methods', *J. Chem. Phys.*, Vol. 81, pp.511–519.

Nosé, S. (1991) 'Constant temperature molecular dynamics methods', *Prog. Theor. Phys. Suppl.*, Vol. 103, pp.1–46.

Oss, C.J.V. (2002) 'Use of the combined Lifshitz-van der Waals and Lewis acid-base approaches in determining the apolar and polar contributions to surface and interfacial tensions and free energies', *Journal of Adhesion Science & Technology*, Vol. 16, No. 6, pp.669–677.

Oss, C.J.V., Chaudhury, M.K. and Good, R.J. (1988) 'Interfacial Lifshitz-van der Waals and polar interactions in macroscopic systems', *Chem. Rev.*, Vol. 88, No. 6, pp.927–941.

Pryatel, J.A., Gourdin, W.H. and Frieders, S.C. (2014) 'Cleaning practices and facilities for the national ignition facility (NIF), laser-induced damage in optical materials', *International Society for Optics and Photonics*, Vol. 9237, p.92372H.

Rubio, F., Rubio, J. and Oteo, J.L. (2000) 'Effect of the measurement temperature on the dispersive component of the surface free energy of a heat treated SiO_2 Xerogel', *Journal of Sol-Gel Science & Technology*, Vol. 18, No. 2, pp.115–118.

Sobczak, N., Singh, M. and Asthana, R. (2005) 'High-temperature wettability measurements in metal/ceramic systems – some methodological issues', *Current Opinion in Solid State and Materials Science*, Vol. 9, Nos. 4–5, p.241.

Stalder, A.F., Kulik, G., Sage, D., Barbieri, L. and Hoffmann, P. (2006) 'A snake-based approach to accurate determination of both contact points and contact angles', *Colloids & Surfaces A: Physicochemical & Engineering*, *Aspects*, Vol. 286, No. 1, pp.92–103.

Stalder, A.F., Melchior, T., Müller, M., Sage, D., Blu, T. and Unser, M. (2010) 'Low-bond axisymmetric drop shape analysis for surface tension and contact angle measurements of sessile drops', *Colloids & Surfaces A: Physicochemical & Engineering Aspects*, Vol. 364, No. 1, pp.72–81.

Sun, D.Y., Asta, M. and Hoyt, J.J. (2004) 'Crystal-melt interfacial free energies and mobilities in fcc and bcc Fe', *Phys. Rev. B*, Vol. 69, No. 17, p.174103.

Sun, H. (1998) 'COMPASS: an ab initio force-field optimized for condensed-phase applications overview with details on alkane and benzene compounds', *J. Phys. Chem. B*, Vol. 102, No. 38, pp.7338–7364.

Sun, H., Ren, P. and Fried, J.R. (1998) 'The COMPASS force field: parameterization and validation for phosphazenes', *Comput. Theor. Poly. Sci.*, Vol. 8, Nos. 1–2, pp.229–246.

Trevoy, D.J. and Johnson Jr., H. (1958) 'The water wettability of metal surfaces', *J. Phys. Chem.*, Vol. 62, No. 7, p.833.

Verlet, L. (1967) 'Computer experiments on classical fluids. I. Thermodynamical properties of Lennard-Jones molecules', *Phys. Rev.*, Vol. 159, pp.98–103.

Wenzel, R.N. (1936) 'Resistance of solid surfaces to wetting by water', *Industrial & Engineering Chemistry*, Vol. 28, No. 8, pp.988–994.

Yin, J. and Cao, Y. (2019) 'Research of laser-induced damage of aluminum alloy 5083 on micro-arc oxidation and composite coatings treatment', *Optics Express*, Vol. 27, No. 13, p.18232.

Yin, J., Cao, Y. and Yan, Y. (2020) 'Laser-induced damage of black glass before and after surface treatment by containing impurities-SiO_2 film during ultra clean manufacturing', *Journal of Cleaner Production*, Vol. 257, p.120360.

Zhao, Y.P. (2002) 'Morphological stability of epitaxial thin elastic films by van der Waals force', *Archive of Applied Mechanics*, Vol. 72, No. 1, pp.77–84.

Appendix 1

Example for the water-aluminium interface model

Figure A1 Atomic model for the water-aluminium interface: H_2O-Al(1 0 0) is taken as an example, and Al, H, and O atoms are represented using purple, white, and red colours, respectively (see online version for colours)

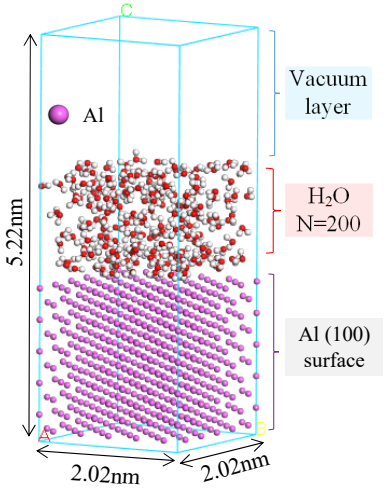

Appendix 2

Contact angle tests with elevated surface roughness

Firstly, the stainless steel 304 (with main element Fe) and aluminium alloy 6061 (with main element Al) with various surface roughness are under a same clean treatment process with temperature 296 K and 45% RH. After that, the contact angles were tested for both samples, the results are as shown in Figure A2.

Figure A2 The experimental contact angle as functions of surface roughness (see online version for colours)

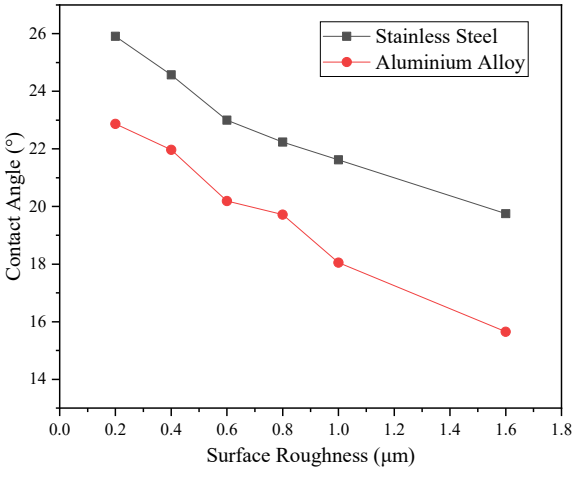

The contact angle of real solid surface with roughness can be explained using Wenzel (1936) model, in which the surface roughness are considered to enlarge the real contact surface, then influence the real contact angle value, and the equation for Wenzel model is as follows.

$$\cos\theta^* = r\cos\theta \tag{A1}$$

where θ^* is the real contact angle, θ is the Young's contact angle, and r is the Wenzel surface roughness.

It can be found from our test that for contact angles $\theta < 90°$, the contact angle of both samples reduce with elevated surface roughness, which match with the Wenzel model.